Drug retention after intradiscal administration

Imke Rudnik-Jansen, Jie Du, Nina Karssemakers-Degen, Anna R. Tellegen, Parvesh Wadhwani, Daniele Zuncheddu, Björn P. Meij, Jens Thies, Pieter Emans, Fetullah C. Öner, George Mihov, Joao Pedro Garcia, Anne S. Ulrich, Sibylle Grad, Marianna A. Tryfonidou, Hugo van Ingen & Laura B. Creemers

View supplementary material

Published online: 20 Oct 2024.

Submit your article to this journal

Article views: 318

View related articles

View Crossmark data

Taylor & Francis
Taylor & Francis Group

RESEARCH ARTICLE

Drug retention after intradiscal administration

Imke Rudnik-Jansen[a,b,c], Jie Du[a], Nina Karssemakers-Degen[d], Anna R. Tellegen[e], Parvesh Wadhwani[f], Daniele Zuncheddu[g], Björn P. Meij[e], Jens Thies[d], Pieter Emans[h], Fetullah C. Öner[a], George Mihov[d], Joao Pedro Garcia[a], Anne S. Ulrich[f], Sibylle Grad[g], Marianna A. Tryfonidou[e], Hugo van Ingen[i] and Laura B. Creemers[a]

[a]Department of Orthopedics, University Medical Center Utrecht, Utrecht, The Netherlands; [b]Department Anesthesiology and Pain Management, Maastricht University Medical Center (MUMC+), Maastricht, The Netherlands; [c]Department Translational Neuroscience, School of Mental Health and Neuroscience (MHeNs), University of Maastricht, Maastricht, The Netherlands; [d]DSM Biomedical, Geleen, The Netherlands; [e]Department of Clinical Sciences, Faculty of Veterinary Medicine, Utrecht University, Utrecht, The Netherlands; [f]Institute of Biological Interfaces (IBG2) and Institute of Organic Chemistry (IOC), Karlsruhe Institute of Technology (KIT), Karlsruhe, Germany; [g]AO Research Institute Davos, Davos, Switzerland; [h]Department of Orthopaedics, Maastricht University Medical Center, Joint-Preserving Clinic Maastricht, The Netherlands; [i]NMR Group, Bijvoet Centre for Biomolecular Research, Utrecht University, Utrecht, The Netherlands

ABSTRACT

Intradiscal drug delivery is a promising strategy for treating intervertebral disk degeneration (IVDD). Local degenerative processes and intrinsically low fluid exchange are likely to influence drug retention. Understanding their connection will enable the optimization of IVDD therapeutics. Release and retention of an inactive hydrophilic fluorine-19 labeled peptide (^{19}F-P) as model for regenerative peptides was studied in a whole IVD culture model by measuring the ^{19}F-NMR (nuclear magnetic resonance) signal in culture media and IVD tissue extracts. In another set-up, noninvasive near-infrared imaging was used to visualize IR-780, as hydrophobic small molecular drug model, retention upon injection into healthy and degenerative caudal IVDs in a rat model of disk degeneration. Furthermore, IR-780-loaded degradable polyester amide microspheres (PEAM) were injected into healthy and needle pricked degenerative IVDs, subcutaneously, and in knee joints with and without surgically-induced osteoarthritis (OA). Most ^{19}F-P was released from the IVD after 7 days. IR-780 signal intensity declined over a 14-week period after bolus injection, without a difference between healthy and degenerative disks. IR-780 signal declined faster in the skin and knee joints compared to the IVDs. IR-780 delivery by PEAMs enhanced disk retention beyond 16 weeks. Moreover, in degenerated IVDs the IR-780 signal was higher over time than in healthy IVDs while no difference between OA and healthy joints was noted. We conclude that the clearance of peptides and hydrophobic small molecules from the IVD is relatively fast. These results illustrate that development of controlled release formulations should take into account the target anatomical location and local (patho)biology.

GRAPHICAL ABSTRACT

HIGHLIGHTS
- Tissue degeneration alters molecule retention in tissues with a low fluid clearance
- Extrapolating retention between different anatomical locations is not recommended
- Drug delivery platforms should be customized to anatomical location
- Drug delivery platforms should be customized to existing pathophysiology

1. Introduction

Chronic low back pain (CLBP) is one of the leading causes of disability (Vos et al., 2016). This painful disability causes functional limitations leading to decreased productivity accompanied by enormous health care costs and a high socio-economic burden (Katz, 2006; Geurts et al., 2018). Degeneration of the intervertebral disk (IVD) has been indicated to be the underlying factor for CLBP in approximately 40% of the cases (Zhang et al., 2009). During the process of IVD degeneration, loss and remodeling of extracellular matrix (ECM) proteins from the macromolecular framework of collagens and proteoglycans will lead to a decrease in water content in the disc (Antoniou et al., 1996; Roughley, 2004). The disorganized and dehydrated IVD in turn will fail to provide the compressive strength that is needed to absorb shocks and to allow movements of the spine (Gruber and Hanley, 2002). Inflammation plays a considerable role in these degenerative processes (Molinos et al., 2015). In addition, the degenerative environment stimulates an increase in local neurotrophic factors leading to the ingrowth of peripheral nociceptive sensory neurons into the IVD, also resulting in pain sensitization (Freemont et al., 1997; Melrose et al., 2002). Anti-inflammatory and analgesic medication is commonly used to relieve pain, such as non-steroidal anti-inflammatory drugs (NSAIDs) and opioids (Enthoven et al., 2017), but long-term use is associated with severe adverse effects such as gastro-intestinal and cardiovascular complications or addiction (Roelofs et al., 2008; Foster et al., 2018). More importantly, systemic drug administration used to treat CLBP remains inefficient, most likely due to the fact that the IVD is the biggest avascular tissue in the human body, and systemically administered drugs hardly reach the tissue (Whatley & Wen, 2012; Tryfonidou et al., 2020). A promising strategy for CLBP treatment could, therefore, be intradiscal delivery of therapeutic molecules. Compared to systemic administration, intradiscal injections will increase local drug concentration and diminish side effects.

Drugs such as peptides have gained interest as therapeutics because of their potential as regenerative agents. Link N peptide consisting of an N-terminal region of link protein stabilizing proteoglycan aggregates, has been shown *in vitro* and *in vivo* to increase disk ECM production necessary to induce tissue regeneration (Petit et al., 2011; Wang et al., 2013; Mwale et al., 2018). Moreover, generally toxicity is low (Muttenthaler et al., 2021), as also confirmed in an *in vivo* study on intradiscal delivery of an NF-κB essential modulator binding domain peptide (Glaeser et al., 2020). However, the systemic half-life of peptides is typically in the range of several minutes, which points to the need for enhancing bioavailaby (Kontermann, 2016). Local injection may delay clearance, but local peptide degradation and clearance rates from the IVD have not been reported. In addition, the use of drug delivery systems (DDS) could be exploited to extend the local exposure of bioactive agents, prolonging discogenic CLBP treatment and/or reversing IVD degeneration (Blanquer et al., 2015). Other promising small-molecule candidates as therapeutic tool for IVD degeneration include microRNAs that have shown to be dysregulated in IVD degeneration (Le Moal et al., 2022), senolytic drugs such as the hydrophobic small-molecule navitoclax (Lim et al., 2022) or targets in the secretory autophagy pathway such as synthetic growth hormone-releasing hormone analog MR409 (Zheng et al., 2021). The direct injection of small-molecule drugs could be a convenient delivery method, but the effect would typically be short-lived due to fast degradation. Drug delivery platforms can protect oligonucleotide-based therapeutics from exposure to local endonucleases or ensure prolonged therapeutic effects of other small-molecule drugs (e.g. protein-based drugs). Injectable hydrogels (Bao et al., 2023; Bhujel et al., 2023; Suzuki et al., 2023) are often preferred as carrier due to the biochemical

properties that are similar to the disk ECM. Other state-of-the-art delivery systems include nanostructures (Wagner et al., 2020) and biodegradable microspheres (Yuan et al., 2023)

Delivery of small molecule anti-inflammatory drugs by polyesteramides (PEAs) *in vivo* has shown promising inhibition of the local inflammation (Janssen et al., 2016; Peters et al., 2017; Tellegen et al., 2018; Rudnik-Jansen et al., 2019). PEAs are biodegradable polymers consisting of natural α-amino acids that can be used as microsphere DDS (Janssen et al., 2016; Tellegen et al., 2018). PEA is broken down into nontoxic waste products by proteolytic enzymes (Botines et al., 2006) and shows good biocompatibility in knee joints (Janssen et al., 2016) and the IVD (Willems et al., 2017). This was exemplified in a puncture-induced canine disk degeneration model administering the anti-inflammatory drug celecoxib intradiscal using PEA microspheres (Tellegen et al., 2018). Furthermore, it reduced owner-reported pain signs at 6 and 12 weeks follow-up in a small cohort of canine CLBP patients (Wiersema et al., 2021). However, in order to develop optimal formulations for the local delivery of bio-actives, insight into local clearance kinetics is required.

Drug distribution and retention in tissue after local administration can be investigated by invasive methods such as mass spectrometry (Gaudreault et al., 2005; Cuyckens, 2019) and little or noninvasive methods, including enzyme-linked immunosorbent assay (ELISA) and imaging based on fluorophore-labeling (Normand et al., 2020). Noninvasive methods can longitudinally track drugs when labeled with a tracer such as a near infrared fluorescent dye. Weak tissue penetration of these dyes usually limits their use in deep tissue locations like the lumbar IVD, and are limited to small animal models. In contrast, invasive methods are normally performed *postmortem,* are highly sensitive and often do not require specific drug labeling. However, quantitative analysis of peptides and proteins in living tissue over time is a challenge due to their inherent instability. In this respect,[19]Fluorine nuclear magnetic resonance (^{19}F NMR) spectroscopy is a highly specific tool for detecting, identifying, and quantifying fluorine-containing drugs and their metabolites in bio-fluids without interference by endogenous components (Malet-Martino et al., 2006)

The present study used invasive and noninvasive tracking methods to investigate drug retention after intradiscal injection (Figure 1). To this end, ^{19}F NMR spectroscopy was here used for the first time to investigate peptide release and retention after intradiscal injection into whole bovine caudal IVDs cultured with dynamical loading. Real-time monitoring of drug presence can be done using noninvasive imaging techniques such as near-infrared (NIR) imaging (Reum Son et al., 2015; Rudnik-Jansen et al., 2017). Another advantage of using NIR imaging to assess local small-molecule release, albeit released from delivery systems, is the minimal tissue auto-fluorescence in the NIR wavelength region (Weissleder & Ntziachristos, 2003). Therefore, noninvasive near-infrared (NIR) imaging was used as this uniquely allows following drug retention over time without sacrificing animals. To this end, the NIR dye IR-780 as model for hydrophobic small molecules, was locally injected in healthy and degenerative caudal rat IVDs to determine the effect of a local disease process. Furthermore, IR-780 was loaded into PEA microspheres to determine drug

retention after injection in healthy and degenerated IVDs. Several regenerative therapies aimed to restore cartilaginous structures have been proposed for knee osteoarthritis (OA) as well as IVD degeneration (Richardson et al., 2016) due to the similarities in tissue composition and degenerative processes (Fine et al., 2023). Therefore, intradiscal IR-780 release profiles from PEA microspheres were also compared to the release profiles in OA knee joints, healthy knee joints and the skin.

2. Materials and methods

2.1. Peptide and microsphere preparations

For NMR based tracking of peptide retention, a peptide (^{19}F-P) consisting of 16 amino acids in a random, unstructured hydrophilic sequence, containing multiple fluorine-19 labels [CF$_3$CO–NH-Lys–(CO–CF$_3$)-DNRAHLHIDYHTDSD-COOH] was purchased from CanPeptide (Canada). Polyesteramine (PEA) III Ac Bz was synthesized (Tsitlanadze et al., 2004; Tellegen et al., 2018) and used to prepare IR-780 dye-loaded microspheres. PEA was dissolved in dichloromethane (DCM, Merck Millipore, Darmstadt, Germany) and IR-780 iodide (425311, Sigma-Aldrich, Darmstadt, Germany) was added to the solution and homogenized by ultrasound. The homogenized suspension was added to 20 mL of an aqueous solution containing surfactants for stabilization (1 wt% of poly(vinyl alcohol and 2.5 wt% NaCl, Sigma Aldrich)) and emulsified under high shear, using an Ultra-Turrax. Thereafter, the particles were allowed to harden overnight in 100 mL water. The excess water and surfactant were removed by rinsing and centrifugation. Before freeze-drying to remove residuals, particles were resuspended in 0.04% Tween 80 and contained final loading of 2 wt% IR-780. Once dried, closed vials were sterilized with γ-radiation on dry ice. The size distribution of PEA particles was measured by static light scattering using a Malvern Mastersizer 2000S and ranged from 8 to 50 μm.

2.2. [19]F peptide retention in bovine IVD ex vivo culture

Bovine caudal IVDs were collected from freshly sacrificed 6- to 12-month-old calves from a local slaughterhouse and whole IVDs with cartilaginous endplates were obtained (Du et al., 2020). The surrounding muscle and soft tissues of the tail was removed, then whole IVDs with cartilaginous endplates were isolated, and redundant vertebral bone were cut off using a band saw and growth plates were carefully scraped off using a scalpel. After cleaning and washing, IVDs were cultured at the free swelling condition in a 6-well plate containing 7 mL culture medium per well and subjected to daily dynamic uniaxial loading in chambers containing 5 mL culture medium at 37 °C, 5% CO$_2$. The culture medium was prepared using high-glucose DMEM (12100061, Gibco), supplemented with 1 mM sodium pyruvate (P5280, Sigma-Aldrich), 50 mM sodium hydrogen carbonate (S5761, Sigma-Aldrich), 2.5% HEPES buffer (15630080, Gibco), 100 U/ mL penicillin and 100 mg/mL streptomycin (15140122, Gibco), 50 mg/mL Primocin (ant-pm, InvivoGen), 2% fetal bovine serum (P30-3306, PAN Biotech), 50 μg/mL ascorbate 2-phosphate (49752, Sigma-Aldrich), 1% ITS+ (354352, BD
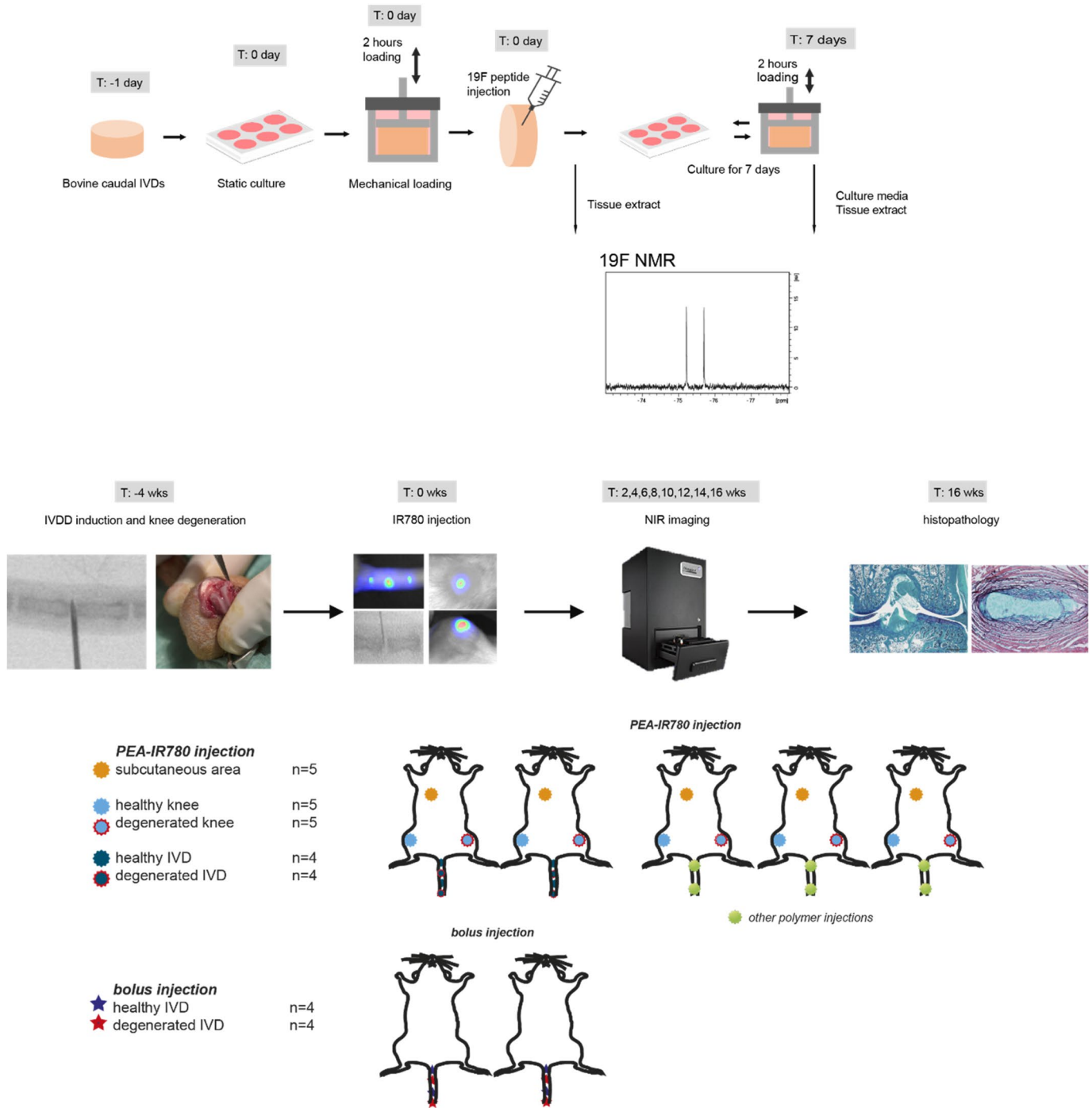
Figure 1. Schematic overview of the study designs including *ex vivo* bovine IVD explants and *in vivo* rat study. IVD: intervertebral disk; IVDD: intervertebral disk degeneration; NIR: near-infrared; PEA: polyesteramide.

Biosciences), and 1% nonessential amino acid (11140050, Gibco) (Lang et al., 2018). IVDs were cultured at the free swelling condition before and after the loading cycle. Dynamic loading was performed at 0.02–0.2 MPa amplitude, 0.2 Hz for 2 hours daily to mimic physiologic loading (Illien-Jünger et al., 2010). After the first loading cycle, 6 IVDs were immediately injected with 1 mg ^{19}F peptide dissolved in 50 μL PBS into the center NP. Then, 3 IVDs were kept in an empty culture plate for 3 hours and harvested as fresh injection control, and another 3 IVDs were cultured under daily mechanical loading for 7 days. Culture media from free swelling and loading systems were collected every day. After 7 days of culture, the endplate of one side of the IVDs was carefully removed, and the IVD was snap-frozen in liquid nitrogen and stored at −20 °C.

2.3. In vivo retention

2.3.1. Ethics statement

The *in vivo* study designs were approved by the National Commission of animal experiments (AVD108002015282), and the working protocol was supervised by the local Animal Welfare Body (WP#105078-2) and (WP#282-5-02) and met the guidelines for animal research in the Netherlands.

2.3.2. In vivo IR-780 retention in rat IVDD and OA

Eight 10-week-old female Sprague-Dawley rats (Charles River Laboratories International, the Netherlands) were used and housed in groups in polycarbonate cages with wire tops, wood chip bedding, and access to *ad libitum* food and tap water. Rats were allowed to acclimatize for 7 days before the start of the experiment. One rat died at $t=0$ directly after IR-780 injection (cause of death; not recovered from anesthesia) and could not be included in the study. The experimental unit in this study was a single injection site for every tissue (PEA-IR780 skin $n=5$, PEA-IR780 healthy knee $n=5$, PEA-IR780 degenerated knee $n=5$, PEA-IR780 healthy IVD $n=4$, PEA-IR780 degenerated IVD $n=4$, free IR-780 healthy IVD $n=4$, free IR-780 degenerated IVD $n=4$). Primary experimental outcomes included IR-780 retention (free or released from PEA microspheres) over time and disk height changes after 16 weeks complemented by histopathology to confirm disk degeneration. Complying with the 3 R principles, 4 rat tails ($n=8$ degenerated IVDs and $n=8$ healthy IVDs) were used to study the IR-780 retention delivered by PEA microspheres, the other 3 for a similar study with a different version of the polymer (unpublished data), which does not influence the present study. IRJ conducted all *in vivo* experiments with the assistance of AT and JPG.

2.3.3. Rat model of induced IVD and knee degeneration

All rats received pre- and post-operatively 0.03 mg/kg buprenorphine (buprecare®) and 4 mg/kg carporal® (AST farma B.V., Oudewater) subcutaneously as prophylactic analgesia. IVD degeneration induction was executed under general anesthesia consisting of isoflurane gas (4–5% induction, 1–2% for maintenance), delivered in a 1:1 oxygen:air mixture. A pre-puncture radiograph (t-4) was taken and used as the baseline for IVD height measurements. Tail IVDs were located by palpation on the coccygeal (Co) vertebrae and confirmed by radiograph. In each animal, IVD degeneration was induced in levels Co4-Co5 and Co6-Co7. Adjacent levels (Co5-Co6 and Co7-Co8) were included as healthy IVD controls. Tail skin was sterilized, and a sterile 20-gauge needle was inserted perpendicular to the skin, at 5 mm depth through the AF into the NP. Correct needle placement was confirmed by intra-operative fluoroscopy. Then, the needle was rotated 360° and held for 30 s (Han et al., 2008). After IVD degeneration induction, the anterior cruciate ligament was transected, and a part of the medial meniscus was removed from the left joint under isoflurane anesthesia (4–5% induction, 1–2% for maintenance). After IVD puncture and knee OA induction, the animals were put back into their cages to recover from surgery. All animals received 0.03 mg/kg buprenorphine subcutaneously as post-operative analgesia for the following three days.

2.3.4. IR-780 injection

IR-780 intradiscal injections (bolus or loaded in PEA microspheres) were performed 4 weeks after degeneration induction (Supplementary Figure 4). All rats received pre-operative analgesia by subcutaneous injection of carprofen (4 mg/kg) and buprenorphine (0.03 mg/kg). All IR-injections were carried out under general anesthesia consisting of isoflurane gas

(4–5% induction, 1–2% for maintenance), delivered in a 1:1 oxygen:air mixture. Before intradiscal injection, radiographs (t_0) were taken to determine changes in IVD height. Then, IR-780 iodide dye alone or IR-780 loaded PEA microparticles were intradiscally injected under fluoroscopic guidance to confirm the correct needle position in the center of the IVD at 625 μg/mL IR-780 in a total volume of 2 μL. Gastight Hamilton syringes (25 μL) connected to 29 G needles (Hamilton Company USA, Reno, Nevada) were used for the intradiscal injections. In the same animals, subcutaneous and intra-articular PEA-IR780 injections were done using 1 mL 29 G insulin needles (Becton Dickson, Franklin Lakes, USA) at a concentration of 625 μg/mL IR-780 in a total volume of 25 μL.

2.4. ^{19}F-NMR spectroscopy

2.4.1. Sample preparation

Frozen ^{19}F-P-injected bovine IVDs were transversely sectioned using a cryostat microtome (Thermo Fisher, USA) at 30 μm thickness. Almost all the NP and AF tissue was sectioned and separately collected. Tissue was lysed in cOmplete lysis-M EDTA-free buffer (Roche Diagnostics GmbH, Mannheim, Germany) on a rotor at 4 °C overnight, around 3 mL per NP and 6 mL per AF. Tissue extracts were collected after centrifuging at 10,000 g at 4 °C for 20 min, then were stored at −80 °C until NMR measurements. Additionally, non-injected fresh bovine IVDs were used to prepare tissue extracts for constructing ^{19}F-P standard for ^{19}F-NMR (Supplementary Figure 2)

Bovine IVD culture media collected daily at days 1–7, were lyophilized, then reconstituted in ultrapure water to concentrate media, 5 times for free swelling media and 4 times for dynamic loading media. Before NMR measurement, 500 μL of each concentrated culture medium and IVD extract was mixed with 50 μL D$_2$O and transferred into 5 mm NMR tube. The standard curve was prepared by dissolving ^{19}F-P at 100 μg/mL, 10 μg/mL, 1 μg/mL in concentrated medium or tissue extract.

2.4.2. ^{19}F-NMR measurements

All ^{19}F-NMR spectra in the bovine IVD extracts and reconstituted culture media were recorded on a Bruker Avance III 600 MHz spectrometer equipped with a Prodigy QCI HFCN quadruple resonance cryo-probe (Billerica, MA). One-dimensional (1D) ^{19}F-NMR spectra were acquired at 298 K using an acquisition time of 2.89 s, recycle delay of 4.5 s, and recording 32 k complex points with a spectral width of 100 ppm centered at −75 ppm. The total recovery delay (7.39 s) was more than 5x the estimated T$_1$ relaxation time, based on analysis of an inversion recovery experiment of ^{19}F-P standard sample (T$_1$ ∼0.7 s). Spectra on media and IVD tissue extracts were recorded using 600 (total acquisition time ∼1 h), while for some IVD samples with weak or no signal, 7200 scans (total acquisition time ∼12 h) were used for bovine IVDs. All spectra were recorded without ^{1}H decoupling, as the ^{19}F-NMR signal in the trifluoromethy-groups of the COCF$_3$ moieties is not affected by ^{19}F-^{1}H couplings. Raw

data were zero-filled to 64 k complex points, and a 2 Hz line broadening window function was applied before Fourier Transformation and subsequent automated phase correction and baseline correction using Bruker Topspin 4.1. Chemical shifts of ^{19}F were referenced with respect to $CFCl_3$ at 0 ppm.

2.4.3. NMR-based quantification

Standard curves were obtained by integrating the signal from −75.0 to −75.8 ppm in tissue samples or −74.9 to −75.7 ppm in media samples, then regressing based on the linear fit as shown in Supplementary Figure 1. The amount of ^{19}F-P in IVDs was calculated by $W_{IVD} = C_{NP} \times V_{NP} + C_{AF} \times V_{AF}$, W_{IVD}: the total amount of ^{19}F-P in IVD, $C_{NP/AF}$: measured ^{19}F-P concentration in NP/AF, $V_{NP/AF}$ volume of lysis buffer added. Accumulated ^{19}F-P release from IVD was calculated by summing the amount of ^{19}F-P in the culture media of each day, which was calculated by $W_M = C_F/5 \times V_F + C_D/4 \times V_D$, W_M: the total amount of ^{19}F-P in culture medium each day, $C_{F/D}$ measured ^{19}F-P concentration in free swelling/dynamic loading medium, $V_{F/D}$ volume of free swelling/dynamic loading medium added.

2.5. Near-infrared imaging

Injection sites (skin, knee joints and tail IVDs) were scanned every other week for *in vivo* IR-780 detection, starting at week 2 after injection. Rats were first sedated by intraperitoneal injection of ketamine (75 mg/kg) and dexmedetomidine (0.25 mg/kg). Images were acquired with the Pearl Impulse Small Animal Imager (LI-COR, Westburg B.V., Leusden, the Netherlands) with 785-nm excitation light to detect IR-780 signal. The Pearl camera automatically optimizes exposure times. Imaging data were acquired with a thermoelectrically cooled CCD sensor. Fluorescence intensity was quantified using Image Studio Lite software (LI-COR, Westburg B.V., Leusden, the Netherlands). Regions of interest were selected using an equal-sized circle, and a mean value was calculated with localized background subtraction analysis. The IR-780 intensity of each time point was normalized to the value of week 2 after injection (100%), as positioning of the animals inside needed to be changed between week 0 and week 2, due to the gain in weight. Unloaded PEA microparticles showed no fluorescence spectra. NIR Imaging was also performed on *postmortem* IVDs after the skin was removed and on paraffin-embedded sections.

2.6. Disk height analysis

Caudal disk radiographs were taken before induction of IVD degeneration ($t-4$) and directly after IR-780 injection (t0). The rats were placed in the prone position with their tails straight during radiography. IVD height was measured using the digital radiographs in Adobe Photoshop software (Adobe Systems Incorporated, version 13.0.1, San Jose, CA) using the ruler tool. IVD height was expressed as the disk height index (DHI) by averaging the measurements obtained from the dorsal, middle, and caudal portions of the IVD and dividing that by the average of adjacent vertebral body heights described by Masuda *et al.* (2005).

2.7. Histopathology

Rats were terminated by CO_2 asphyxiation 16 weeks after degeneration induction on t-4. Tails and knee joints were harvested. Tails were skinned and imaged again before fixation. Tails and knees were fixed in 4% formaldehyde solution (Klinipath B.V., Duiven, the Netherlands) for 1 week. Thereafter, they were decalcified in 0.5 M EDTA (VWR international B.V., Amsterdam, the Netherlands) solution for a total of 6 and 8 weeks, respectively, re-fixing for 3 days in 4% formaldehyde solution every 2 weeks. The IVDs were embedded in paraffin as spinal units containing the adjacent vertebral bodies. Five µm sections were used to take NIR images and stain with Picrosirius red/Alcian blue staining protocols (Gruber et al., 2002). The cellularity and morphology of all IVDs was examined in a random blinded fashion. Five µm thick transversal knee joint sections were cut and stained either with Safranin-O/Fast green or hematoxylin/eosin to evaluate cartilage degeneration using the Mankin score (Mankin & Lippiello, 1970) or synovitis using the Krenn score (Krenn et al., 2006), respectively.

2.8. Statistical analysis

All data were analyzed using IBM® SPSS® Statistics software (version 21). One-Sample *t*-tests were used to analyze the significance of differences in DHI between healthy and degenerated IVDs and cartilage degeneration and synovitis between healthy and degenerated knee joints. All IR-780 fluorescence intensity data were evaluated for equality of data variances by Q-Q plots and homoscedasticity of residuals by scatterplots. In all cases, the assumptions were not met, and Kruskal–Wallis tests were used to analyze nonparametric data with post-hoc pairwise comparisons using the Dunn-Bonferroni approach. All data were expressed as the mean ± standard error of the mean. Statistically significant differences were considered at values $p < 0.05$. Statistical analysis of peptide measurements was limited to descriptive statistics.

3. Results and discussion

Intradiscal delivery of drugs is gaining acceptance as a promising approach to treating CLBP or regenerating IVD as an alternative to systemic administration. In the current study, we investigated the relation between drug retention and the local environment and disease state of the injected tissue by using ^{19}F-P and IR-780 as a model of peptide and small molecule, respectively.

3.1. ^{19}F-peptide clearance from the intervertebral disk

In this study, for the first time, a ^{19}F-labeled peptide was used as an inert model peptide to investigate drug release and retention in the IVD. This was done by using ^{19}F-NMR in an *ex vivo* bovine IVD culture model. The main signals were located at −75.2 and −75.7 ppm in lysis buffer, and a small peak was found between the two main peaks that may indicate free trifluoroacetic anhydride (TFA, Supplementary Figure

1). A chemical shift was found when ^{19}F-P was dissolved in the IVD culture medium and concentrated culture medium, compared to lysis buffer and tissue extracts (Supplementary Figure 1). In the IVD culture model, three hours after injection of 1 mg of ^{19}F-P in bovine IVDs (Figure 2(A)), most ^{19}F-P was found in the NP tissue, which was ~29% of the total dose injected, while only ~4% was detected in AF tissue extracts (Figure 2(B)). Almost 70% could not be recovered from tissue extracts. During culture, ~22% of the injected ^{19}F-P was released to the culture medium in the first 4 days. The cumulative release was 24% after 7 days of culture (Figure 2(C)). After 7 days of culture, less than 1% ^{19}F-P was retrieved from the NP, and nothing from the AF (Figure 2(D)).

In general, peptide drugs have a serum half-life of minutes and hence low bioavailability, due to rapid clearance by the liver or kidney (Ayoub & Scheidegger, 2006). Intradiscal peptide application has been performed in order to increase local drug concentrations and prolong drug retention in rat and rabbit IVDD models, although actual retention was not investigated (Mwale et al., 2018; Glaeser et al., 2020). In the present study, ^{19}F-P could be detected in IVD extracts at μg levels. ^{19}F-NMR was used before to quantify fluoropyrimidine and its metabolites from plasma in rat and dog, showing comparable sensitivity to liquid chromatography with tandem mass spectrometry (Hu et al., 2015). In the current study, according to results of drug release and retention in cultured IVDs the half-life of the locally injected peptide was indeed enhanced compared to serum. Nevertheless, the majority of ^{19}F-P still appears to be cleared from the IVD within one

week. This is in line with a previous study, in which a soluble fluorescent dye, isothiocyanate isomer 1 (FITC), showed a ~90% signal decrease after 4 days of culture. However, this model consisted of a NP explant cultured inside a cartilage ring, using static compression, in addition to the smaller size of the molecule studied (Wagner et al., 2020). Why only one third of ^{19}F-P was recovered from the freshly injected IVDs is unclear. Fractions of the ^{19}F-P might may have diffused to the cartilaginous endplates, which were not analyzed. Also in calculating the total volume of tissue lysate, the volume of the NP/AF tissue itself was not included, and hence the recovered ^{19}F-P could have been underestimated. An alternative explanation could be that ^{19}F-P binds to the insoluble part of the ECM, and hence did not dissolve fully into the tissue extracts that were used to quantify ^{19}F-P. To address this possibility, methods interfering with peptide-ECM interaction should be applied to enable release of the ^{19}F-P into the tissue extract. Interaction with ECM components may likewise also be the reason for observation that the ^{19}F-P content was higher in the NP than in the AF tissue, both in freshly injected IVDs and after 7 days of culture. ^{19}F-NMR can also be used for the detection of peptide metabolites based on their chemical shifts (Hu et al., 2015). In the present study, we did not observe any such new signals in the NP extract after 7 days of culture. This may suggest that a major amount of ^{19}F-P in the IVD was not degraded. Alternatively, we might have missed degradation signals due to the limited sensitivity of the experiments. Also, due to the particular position of the ^{19}F-label in the peptide (at the N-terminus and residue 1) the
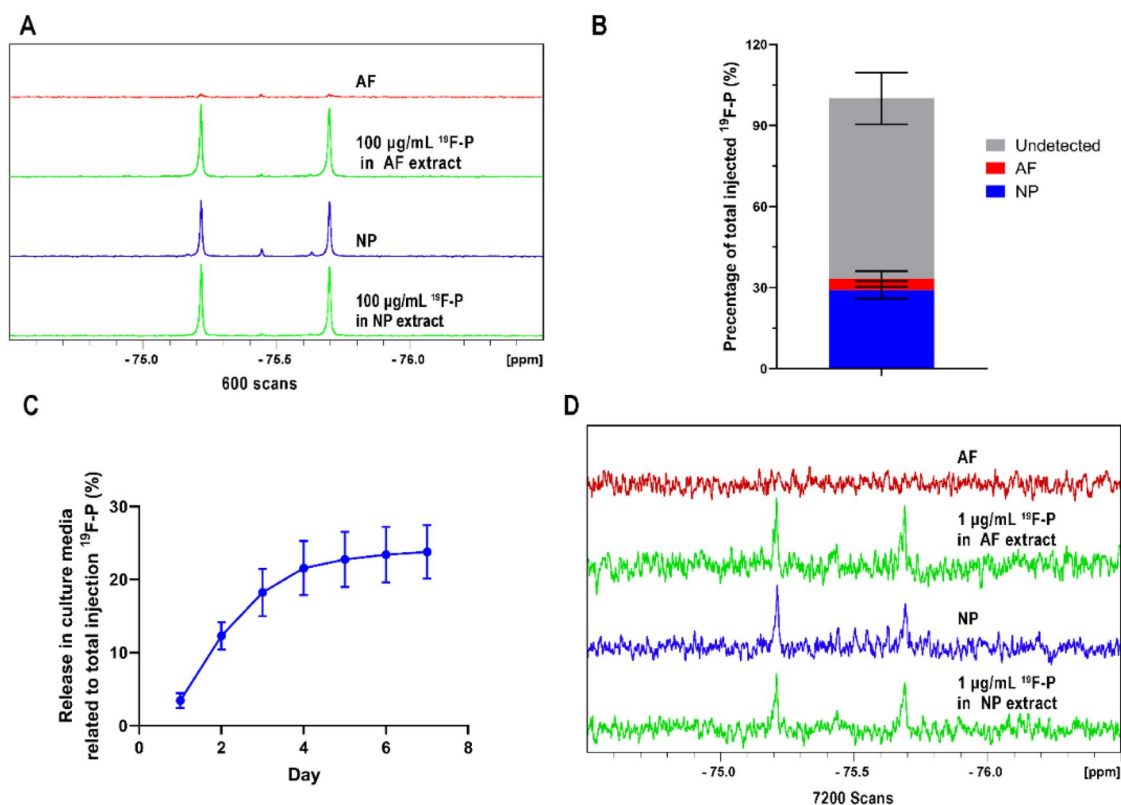

Figure 2. 19F-P release and retention in cultured bovine caudal intervertebral disk (IVD) after intradiscal injection evaluated by nuclear magnetic resonance. (A) Evaluation and (B) quantification of ^{19}F-P in bovine AF and NP tissue extracts, 3 h after intradiscal injection using ^{19}F-NMR spectroscopy. (C) The release profile and (D) retention of ^{19}F-P in bovine caudal IVDs cultured with daily dynamic loading for 7 days after intradiscal injection. AF: annulus fibrosus; NP: nucleus pulposus.

^{19}F signal will not be sensitive to degradation at more C-terminal positions in the peptide.

^{19}F-NMR spectroscopy is only able to measure endpoint read-outs. Noninvasive ^{19}F nuclear magnetic resonance imaging (^{19}F-MRI), on the other hand, would offer *in vivo* detection and tracking of injected substances (Gonzales et al., 2016; Arakawa et al., 2020). ^{19}F-MRI has high specificity due to the lack of endogenous ^{19}F, but is still challenged to date by the low sensitivity of ^{19}F detection and the specialized hardware required. Usually, it requires a local ^{19}F concentration over 80 mM to obtain high-quality images, whereas *in vivo* drug concentrations are usually in the sub-mM range (Bo et al., 2018). Recently, a labeling strategy for *in vivo* ^{19}F-MRI based on highly fluorinated, short hydrophilic peptide probes or drug carriers has been developed (Bo et al., 2018; Meng et al., 2022). Intradiscal delivery of such systems could possibly increase local concentrations enabling real-time detection of drug retention over time, including peptides.

3.2. IR-780 retention in the intervertebral disk

In small animal models, real-time monitoring of drug presence can be done via noninvasive imaging techniques, such as NIR fluorescence imaging (Reum Son et al., 2015; Rudnik-Jansen et al., 2017). Another advantage of using NIR imaging to assess local drug release over time is the minimal tissue autofluorescence in the NIR wavelength region (Weissleder & Ntziachristos, 2003). Percutaneous needle puncture of rat tail IVDs resulted in significant disk space narrowing after 4 weeks, measured prior to intradiscal IR-780 delivery, in comparison with adjacent control disks (Figure 3(A)).

Postmortem histological images confirmed the healthy disk status of the latter, showing normal IVD tissue compositions containing organized collagen lamellae of the AF surrounding a round and notochordal cell-rich NP, which in rodents is the predominant cell type in the healthy NP (Figure 3(B)). The presence of degeneration processes 16 weeks after needle puncture was indicated by disorganized collagen fibers transitioning into the irregularly shaped NP with disrupted endplates (Figure 3(B)).

The retention of free IR-780 after intradiscal delivery gradually declined at a pace that appeared to be independent of the IVD health status (Figure 3 C&D, n.s). The IR-780 signal was below detection 10 weeks after injection in degenerated IVDs, while the detection limit was reached after 14 weeks in healthy IVDs, but this difference was not significant.

3.3. IR-780 delivery and retention using a PEA-based drug delivery platform

PEA microspheres were used as a model of a controlled release platform for local injection. IR-780 retention gradually decreased in the skin and knee joint and was undetectable 16 weeks after injection. In contrast, the IR-780 signal increased in the first 6 weeks after intradiscal injection, and thereafter a slow, gradual decrease was observed (Figure 4 A). IR-780 signal remained visible after the 16 weeks follow-up period, and the relative IR-780 intensity was significantly higher in the IVD compared to the skin and knee joint (Figure 4(A,B), $p < 0.05$).

The retention and inherent release rate of the drug loaded in a DDS depend on the biomaterial-based DDS properties such as porosity, properties of the drug such as size and
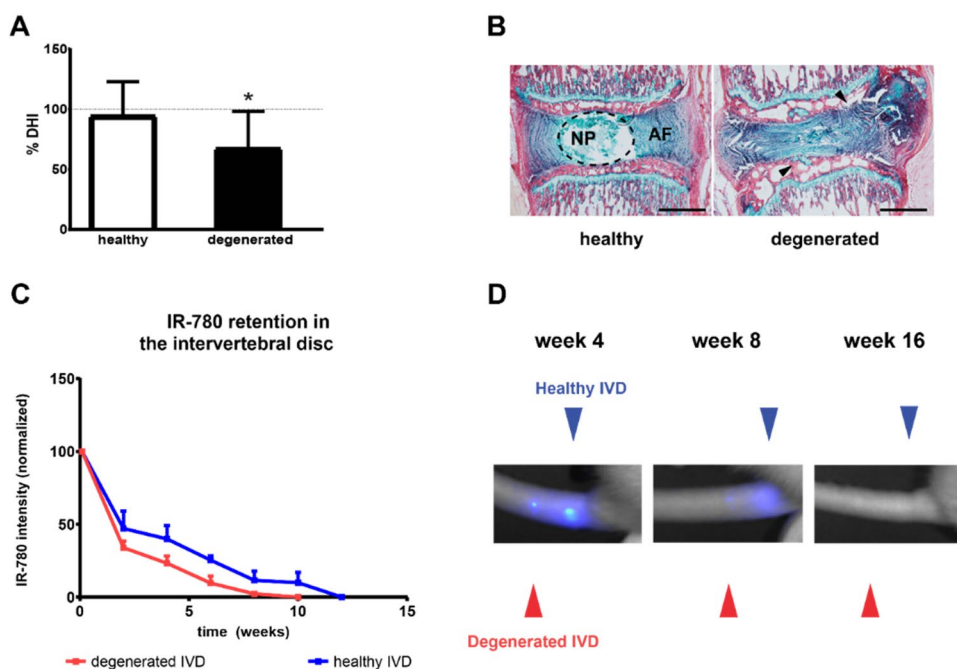

Figure 3. Retention of free IR-780 after intradiscal injection in healthy or degenerated intervertebral disks (IVDs). (A) Decreased disk height index (DHI), 4 weeks after degeneration induction by NP needle puncture. *$p < 0.05$. (B) Histologic overview of a healthy and degenerated IVD, stained with picrosirius red/alcian blue. The dotted circle indicates a distinct NP (left), and black arrows indicate disrupted endplates (right). Scale bar = 500 μm. (C) Quantification of IR-780 intensity signal after IR-780 injection in healthy ($n = 4$) or degenerated ($n = 4$) rat IVDs. The IR-780 intensity was normalized to 2 weeks after injection. Data represent mean ± SEM. (D) IR-780 signal after 4 and 8 weeks in tail IVDs, detected by fluorescence optical imaging. AF: annulus fibrosus; NP: nucleus pulposus.

charge, and on clearance from the injected tissue. In addition, release from the PEA polymer is also enzyme-responsive, being sensitive to serine protease-dependent degradation (Janssen et al., 2016). Various serine proteinases have been described to play a role in (osteo)arthritis and IVD pathology (Wilkinson et al., 2019). In particular, plasmin and HtrA1 have been detected in degenerated IVDs at higher levels compared to healthy IVD tissue (Salo et al., 2008; Tiaden et al., 2012; Meng et al., 2017), explaining the initial increase in NIR intensity in degenerated IVDs. In a synovial joint, the elimination of intra-articularly injected drugs occurs through the synovial membrane (Sterner et al., 2016), while fluid transport in and out of the IVD is regulated by a combination of diffusive and convective transport (Maroudas, 1975; Roberts et al., 1996). The observed differences in the presence of IR-780 as model drug over time could, therefore, partially be explained by the properties of the injected tissues. Tissues rich in lymphatic vessels are the skin and knee (Porter and Charman, 2000; Shi et al., 2014), in contrast to the tightly enclosed IVD (Kliskey et al., 2009). In these locations with an intrinsically higher fluid clearance, IR-780 retention was indeed lower.

3.4. IR780-PEA retention from healthy and degenerated IVD and knee joint

In degenerated IVDs, the course of IR-780 intensity over time was similar to healthy IVDs. Interestingly, the relative IR-780 intensity increased more strongly in degenerated IVDs than in healthy IVDs. Even 16 weeks after injection, the IR-780 intensity did not significantly decrease compared to 2 weeks in degenerative IVDs. This IR-780 intensity pattern was not observed in knee joints, regardless of health status, that showed a gradual decrease over the 16 weeks period (Figure 5(C), n.s. Figure 5(D)).

Postmortem, in IR780-PEA-injected IVDs, IR-780 signal was still detected after 16 weeks follow-up in degenerated disks, although no statistically significant differences were found in IR-780 signal between degenerated and healthy IVDs (supplementary Figure 5(A)). After tissue processing for histological analysis, local IR-780 signals released from PEA microspheres could still be detected in IVD tissue sections (supplementary Figure 5(B)).

Unexpectedly, no difference in IR-780 retention was observed between healthy and degenerated knee joints upon delivery by PEA microspheres, while enhanced clearance of glucocorticoids (Bonanomi et al., 1987) or large molecules such as hyaluronic acid (Fraser et al., 1993) in inflamed joints has been explained by the increased vascular permeability due to synovitis (Simkin & Bassett, 2011). Considering that the current model displays an OA state in which an increase in lymphatic vasculature has been described 12 weeks after induction of degeneration (Shi et al., 2014), differences in IR-780 retention in this time window were expected. In addition, PEA resorption has previously been shown to be enhanced in OA joints, possibly due to the increase in serine protease activity (Janssen et al., 2016). The PEA microsphere platform exploited in the current paper is uniquely sensitive for serine protease dependent degradation. Various serine proteinases such as granzyme B have been described to play a role in (osteo)arthritis pathology (Cawston & Young, 2010), also found to be upregulated in degenerated IVDs (Salo et al., 2008; Tiaden et al., 2012). The differences in serine proteases present in the tissues might contribute to the differences of IR-780 signal that was observed. Although a trend was observed toward a faster clearance during the first 12 weeks after OA induction in knee joints, the current study may have been underpowered to detect statistically significant differences. For IVD tissues, we did detect a significant higher IR-780 signal and retention between healthy and degenerated IVDs. In contrast to the knee joints and the skin, the IR-780 signal in IVDs increased during the first weeks after intradiscal injection. Moreover, this increase was more pronounced in degenerated IVDs compared to the healthy tissues, where IR-780 signal intensity showed a more gradual increase. The extent of fluid exchange plays an important role in determining local IR-780 retention, as was shown in an elegant finite element model predicting that degenerative changes of the IVD (such as blood supply, endplate permeability, disk geometry or matrix and cellular properties) can impair effects on the concentration gradients of nutrients and metabolites throughout the disc (Sélard et al., 2003) which might also apply for drug retention in the disk. IVD degeneration accompanied by disk deformation results in lower fluid exchange rates, which
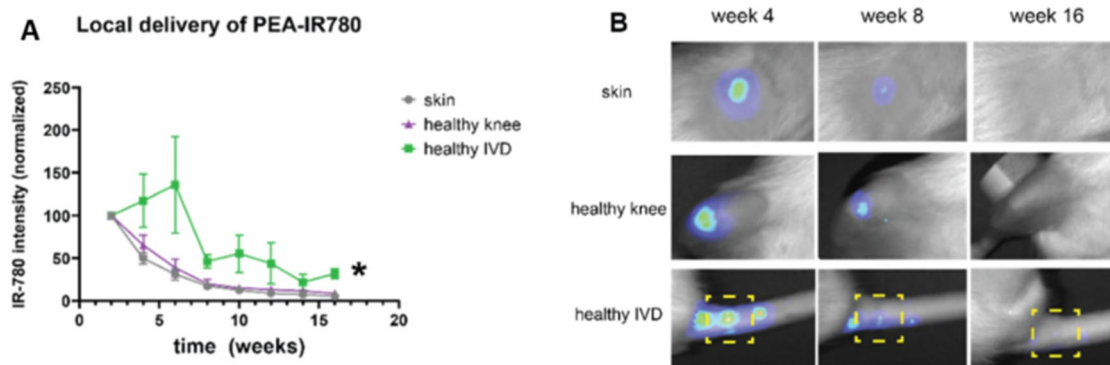

Figure 4. Tissue-dependent retention of IR-780 released from polyesteramide (PEA) microspheres over 16 weeks. (A) Quantification of IR-780 intensity signal after IR-780 injection in healthy skin ($n = 5$), knee joint ($n = 5$), and IVD ($n = 4$). The IR-780 intensity was normalized to the signal 2 weeks after injection. Data represent mean ± SEM. A significant increase in IR-780 intensity was found in IVD compared to skin and knee joints, indicated by *$p < 0.05$. (B) Fluorescence optical images 4 and 8 weeks after IR-780 loaded PEA microsphere injections in rats. The yellow dotted box indicates healthy IVD. IVD: intervertebral disk.
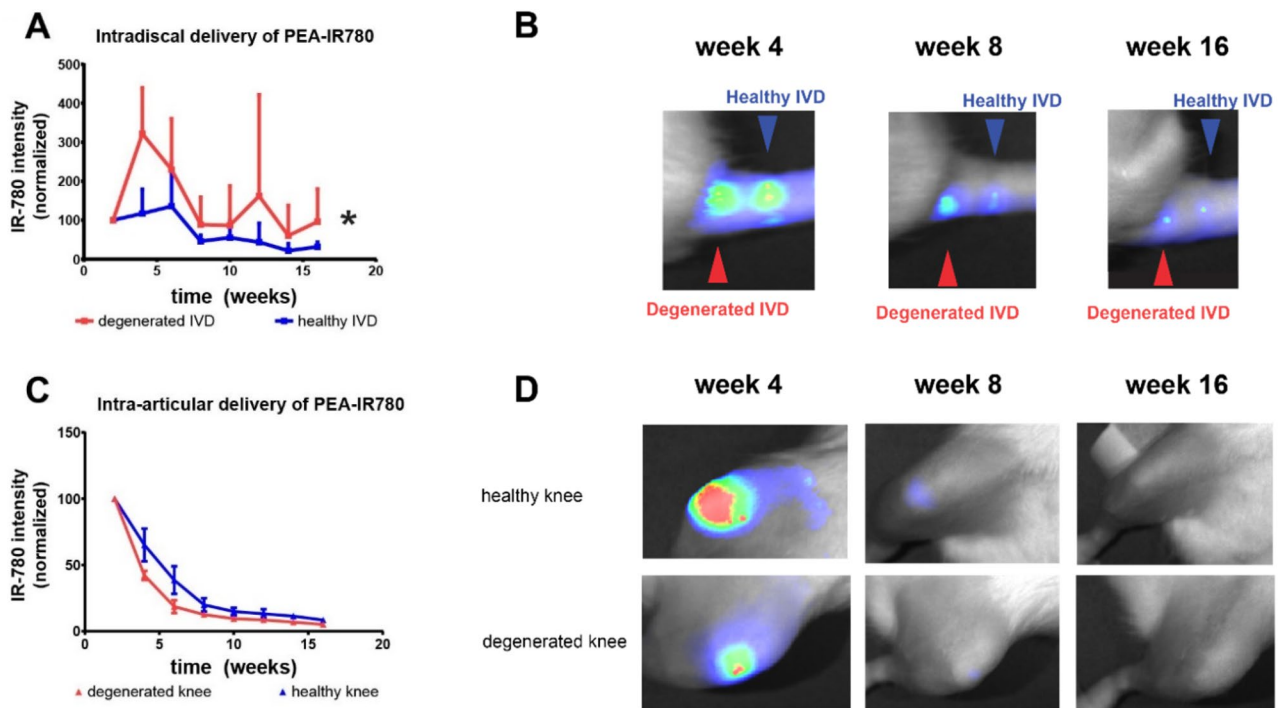
Figure 5. Disease-dependent joint retention of IR-780 over 16 weeks, released from polyesteramide (PEA) microspheres in rats. (A) Quantification of IR-780 signal after IR-780 loaded PEA microsphere (PEA-IR780) injection in healthy IVDs ($n=4$) versus degenerated IVDs ($n=4$) in rats. NIR intensity was normalized to 2 weeks after injection. Data represent mean ± SEM. A significant increase of IR-780 intensity released from PEA microspheres was found in degenerated IVDs compared to healthy IVDs (*$p < 0.05$). (B) Fluorescence optical images 4 and 8 weeks after PEA-IR780 injections in healthy and degenerated tail IVDs in rats. The blue arrows indicate healthy IVD, the red arrows indicate degenerated IVD. (C) Quantification of IR-780 intensity signal after PEA-IR780 injection in healthy knee joints ($n=5$) versus degenerated knee joints ($n=5$). The IR-780 intensity was normalized to 2 weeks after injection. Data represent mean ± SEM, and no significant differences were found. (D) Fluorescence optical images 4 and 8 weeks after PEA-IR780 injections in healthy and degenerated knee joints in rats. IVDs: intervertebral disks.

might lead to a lower clearance and hence may explain higher retention in degenerated IVDs, compared to healthy IVDs (Zhu et al., 2014). In contrast, hypervascularization is one of the degenerative processes occurring in knee joints that will increase the exchange of fluids and thus drug local clearance.

The increase in IR-780 signal upon release in the IVDs can be explained by the phenomenon that a high IR-780 dye molar content in drug delivery systems can induce quenching inside the microparticles, leading to a signal increase upon their release into the tissue (Li et al., 2017). Due to the relatively fast clearance in the knee joint and skin, IR-780 quenching could probably not lead to a signal increase at these locations. The increased IR-780 peak signal in degenerated IVDs compared to healthy IVDs, was most likely due to increased levels of serine proteases in degenerated IVDs (Tiaden et al., 2012), enhancing PEA microsphere degradation (Janssen et al., 2016)

Although the use of IR-780 dye can provide a general insight into local delivery and retention, determining the half-life of IR-780 upon intradiscal injection is not possible, not only due to likely quenching inside the microparticles, but also because it is not known whether the signal and NIR quantity in the IVD are linearly correlated. To this end, non-quenching NIR labels are available to be combined with standard curves in rat caudal IVDs. However, still considerable differences in release are likely to be expected between separate small hydrophobic drugs, based on their physicochemical properties. Labeling the drug of interest with a

radioisotope may provide a clearer insight, although isotope labeling of small molecule drugs is challenging. In this study, the first time point of IR-780 signal intensity measurement was at two weeks post-injection for practical reason (Peters et al., 2017). As a consequence, other phenomena, including a sharp decrease in NIR signal due to an early burst release, may have been missed. However, still the differences in signal loss between degenerated and healthy IVDs remain, suggesting a clear effect of the presence of disease on release of the molecule.

The degenerative processes in an osteoarthritic joint and the IVD are quite similar (Rustenburg et al., 2018), but here we show that drug retention upon local delivery is most likely not comparable. Therefore, the many drug delivery formulations that are being developed to improve therapies for various musculoskeletal conditions should be tailored to the specific needs per disease and anatomical location. Modifications that might improve drug delivery for a specific condition can influence the degradation properties of the polymer. For example, cleavage sites of specific serine proteases might be incorporated into the polymer to increase the sensitivity of the predominant degenerative processes in the target tissue.

4. Conclusions

Direct injection of small molecules, such as peptides or IR-780 iodide, in the IVD increased their systemic half-life and appeared dependent on IVD health status. Despite the

confined space of the IVD, bolus injections of small molecules have shown to be lost relatively fast. Using a drug delivery platform to sustain drug release, small molecule retention was prolonged in the IVD compared to other anatomical locations. The PEA microsphere platform has the potency to provide therapeutic efficacy by the incorporated drugs for over 12 weeks, as was exemplified in a prospective evaluation of local sustained release of small-molecule drug celecoxib in dogs with low back pain (Wiersema et al., 2021). However, investigation of local safety issues of the injected drugs is warranted as extended drug presence could have detrimental effects in certain degenerated joints (Rudnik-Jansen et al., 2019). Nevertheless, IR-780 release and retention from this drug delivery platform appeared to be disease-dependent, which was not the case for the knee joint. Therefore, extrapolation of drug retention patterns from one type of tissue to another type of tissue is not recommended and discourages applying a regenerative therapy for several musculoskeletal diseases (e.g. knee OA and IVD degeneration), despite their similarities in tissue composition and disease progression. Tailoring drug delivery systems would be advised, for example, targeting an avascular IVD with a confined space might benefit from PEA-based microspheres with a more accelerated degradation pace than a knee joint with a relatively higher fluid exchange.

Acknowledgments

Authors contributions

LC, MT, JT, AU, GM, SG, BM conceptualized the experiments. LC, SG, HvI, NKD, PW provided study materials. IRJ, JD, NKD were responsible for data curation. IRJ and JD analyzed and/or synthesized study data and were responsible for data validation. LC, SG, MT supervised the experiments. LC acquired financial support for the project and was responsible for project administration. IRJ, JD, NKD, JPG, AT, PW, DZ, HvI conducted the experiments and/or data collection. IRJ, JD, HvI contributed to visualization and/or data presentation. IRJ, JD, HvI, NKD prepared the original draft. All authors have read, reviewed and agreed to the published version of the manuscript and agreed to be accountable for all aspects of the work.

Disclosure statement

The authors from DSM have proprietary and commercial interest in material discussed in this article. Employer DSM participated as cofinancing R&D partner in the public-private partnership project ArIADNE, in the course of which the in vivo experiments described in the manuscript were performed. DSM had no oversight, influence on decision to publish, nor on content of any part of the publication. All other authors have no conflict of interest.

Funding

References

Antoniou J, Steffen T, Nelson F, et al. (1996). The human lumbar intervertebral disc: evidence for changes in the biosynthesis and denaturation of the extracellular matrix with growth, maturation, ageing, and degeneration. J Clin Invest 98:996–1003. doi:10.1172/JCI118884.

Arakawa H, Yamada H, Arai K, et al. (2020). Possible utility of peptide-transporter-targeting [(19)F]dipeptides for visualization of the biodistribution of cancers by nuclear magnetic resonance imaging. Int J Pharm 586:119575. doi:10.1016/j.ijpharm.2020.119575.

Ayoub M, Scheidegger Chimica Oggi. (2006). Peptide drugs, overcoming the challenges, a growing business. 24:46–48.

Bao J, Gao W, Zhang W, et al. (2023). Fibrin glue delivery system containing rhein ameliorates intervertebral disc degeneration by anti-inflammatory efficacy. J Orthop Surg Res 18:485. doi:10.1186/s13018-023-03961-9.

Bhujel B, Yang SS ,Kim HR, et al. (2023). An injectable engineered cartilage gel improves intervertebral disc repair in a rat nucleotomy model. Int J Mol Sci 24. 3146 doi:10.3390/ijms24043146.

Blanquer SB, Grijpma DW, Poot AA. (2015). Delivery systems for the treatment of degenerated intervertebral discs. Adv Drug Deliv Rev 84:172–87. doi:10.1016/j.addr.2014.10.024.

Bonanomi MH, Velvart M, Stimpel M, et al. (1987). Studies of pharmacokinetics and therapeutic effects of glucocorticoids entrapped in liposomes after intraarticular application in healthy rabbits and in rabbits with antigen-induced arthritis. Rheumatol Int 7:203–12. doi:10.1007/BF00541378.

Bo S, Yuan Y, Chen Y, et al. (2018). In vivo drug tracking with (19)F MRI at therapeutic dose. Chem Commun 54:3875–8. doi:10.1039/c7cc09898g.

Botines E, Franco L, Puiggalí J. (2006). Thermal stability and degradation studies of alternating poly(ester amide)s derived from glycolic acid and omega-amino acids. J Appl Polymer Sci 102:5545–58. doi:10.1002/app.24725.

Cawston TE, Young DA. (2010). Proteinases involved in matrix turnover during cartilage and bone breakdown. Cell Tissue Res 339:221–35. doi:10.1007/s00441-009-0887-6.

Cuyckens F. (2019). Mass spectrometry in drug metabolism and pharmacokinetics: current trends and future perspectives. Rapid Commun Mass Spectrom 33 Suppl 3:90–5. doi:10.1002/rcm.8235.

Du J, Pfannkuche J-J, Lang G, et al. (2020). Proinflammatory intervertebral disc cell and organ culture models induced by tumor necrosis factor alpha. JOR Spine. 3:e1104. doi:10.1002/jsp2.1104.

Enthoven WTM, Roelofs PD, Koes BW. (2017). NSAIDs for chronic low back pain. JAMA 317:2327–8. doi:10.1001/jama.2017.4571.

Fine N, Lively S, Séguin CA, et al. (2023). Intervertebral disc degeneration and osteoarthritis: a common molecular disease spectrum. Nat Rev Rheumatol 19:136–52. doi:10.1038/s41584-022-00888-z.

Foster NE, Anema JR, Cherkin D, et al. (2018). Prevention and treatment of low back pain: evidence, challenges, and promising directions. Lancet 391:2368–83. doi:10.1016/S0140-6736(18)30489-6.

Fraser JR, Kimpton WG, Pierscionek BK, Cahill RN. (1993). The kinetics of hyaluronan in normal and acutely inflamed synovial joints: observations with experimental arthritis in sheep. Semin Arthritis Rheum 22:9–17. doi:10.1016/s0049-0172(10)80015-0.

Freemont AJ, Peacock TE, Goupille P, et al. (1997). Nerve ingrowth into diseased intervertebral disc in chronic back pain. Lancet 350:178–81. doi:10.1016/s0140-6736(97)02135-1.

Gaudreault J, Fei D, Rusit J, et al. (2005). Preclinical pharmacokinetics of Ranibizumab (rhuFabV2) after a single intravitreal administration. Invest Ophthalmol Vis Sci 46:726–33. doi:10.1167/iovs.04-0601.

Geurts JW, Willems PC, Kallewaard JW, et al. (2018). The impact of chronic discogenic low back pain: costs and patients' burden. Pain Res Manag 2018:4696180. doi:10.1155/2018/4696180.

Glaeser JD, Salehi K, Kanim LEA, et al. (2020). NF-κB inhibitor, NEMO-binding domain peptide attenuates intervertebral disc degeneration. Spine J 20:1480–91. doi:10.1016/j.spinee.2020.04.025.

Gonzales C, Yoshihara HAI, Dilek N, et al. (2016). In-vivo detection and tracking of T cells in various organs in a melanoma tumor model by 19F-fluorine MRS/MRI. PLoS One 11:e0164557. doi:10.1371/journal.pone.0164557.

Gruber HE, Hanley ENJr. (2002). Ultrastructure of the human intervertebral disc during aging and degeneration: comparison of surgical and control specimens. Spine (Phila Pa 1976) 27:798–805. doi:10.1097/00007632-200204150-00004.

Gruber HE, Ingram J, Hanley ENJr. (2002). An improved staining method for intervertebral disc tissue. Biotech Histochem 77:81–3.

Han B, Zhu K, Li F-C, et al. (2008). A simple disc degeneration model induced by percutaneous needle puncture in the rat tail. Spine (Phila Pa 1976) 33:1925–34. doi:10.1097/BRS.0b013e31817c64a9.

Hu H, Huang N, Yi P, et al. (2015). Utilizing 19F NMR to investigate drug disposition early in drug discovery. Xenobiotica 45:1081–91. doi:10.3109/00498254.2015.1040866.

Illien-Jünger S, Gantenbein-Ritter B, Grad S, et al. (2010). The combined effects of limited nutrition and high-frequency loading on intervertebral discs with endplates. Spine (Phila Pa 1976) 35:1744–52. doi:10.1097/BRS.0b013e3181c48019.

Janssen M, Timur UT, Woike N, et al. (2016). Celecoxib-loaded PEA microspheres as an auto regulatory drug-delivery system after intra-articular injection. J Control Release 244:30–40. doi:10.1016/j.jconrel.2016.11.003.

Katz JN. (2006). Lumbar disc disorders and low-back pain: socioeconomic factors and consequences. J Bone Joint Surg Am 88 Suppl 2:21–4. doi:10.2106/JBJS.E.01273.

Kliskey K, Williams K, Yu J, et al. (2009). The presence and absence of lymphatic vessels in the adult human intervertebral disc: relation to disc pathology. Skeletal Radiol 38:1169–73. doi:10.1007/s00256-009-0770-2.

Kontermann RE. (2016). Half-life extended biotherapeutics. Expert Opin Biol Ther 16:903–15. doi:10.1517/14712598.2016.1165661.

Krenn V, Morawietz L, Burmester G-R, et al. (2006). Synovitis score: discrimination between chronic low-grade and high-grade synovitis. Histopathology 49:358–64. doi:10.1111/j.1365-2559.2006.02508.x.

Lang G, Liu Y, Geries J, et al. (2018). An intervertebral disc whole organ culture system to investigate proinflammatory and degenerative disc disease condition. J Tissue Eng Regen Med 12:e2051–e2061. doi:10.1002/term.2636.

Le Moal B, Lepeltier É, Rouleau D, et al. (2022). Lipid nanocapsules for intracellular delivery of microRNA: a first step towards intervertebral disc degeneration therapy. Int J Pharm 624:121941. doi:10.1016/j.ijpharm.2022.121941.

Lim S, An SB, Jung M, et al. (2022). Local delivery of senolytic drug inhibits intervertebral disc degeneration and restores intervertebral disc structure. Adv Healthc Mater 11:e2101483. doi:10.1002/adhm.202101483.

Li S, Johnson J, Peck A, Xie Q. (2017). Near infrared fluorescent imaging of brain tumor with IR780 dye incorporated phospholipid nanoparticles. J Transl Med 15:18. doi:10.1186/s12967-016-1115-2.

Malet-Martino M, Gilard V, Desmoulin F, Martino R. (2006). Fluorine nuclear magnetic resonance spectroscopy of human biofluids in the field of metabolic studies of anticancer and antifungal fluoropyrimidine drugs. Clin Chim Acta 366:61–73. doi:10.1016/j.cca.2005.10.013.

Mankin HJ, Lippiello L. (1970). Biochemical and metabolic abnormalities in articular cartilage from osteo-arthritic human hips. J Bone Joint Surg Am 52:424–34.

Maroudas A. (1975). Biophysical chemistry of cartilaginous tissues with special reference to solute and fluid transport. Biorheology 12:233–48. doi:10.3233/bir-1975-123-416.

Masuda K, Aota Y, Muehleman C, et al. (2005). A novel rabbit model of mild, reproducible disc degeneration by an anulus needle puncture: correlation between the degree of disc injury and radiological and histological appearances of disc degeneration. Spine (Phila Pa 1976) 30:5–14. doi:10.1097/01.brs.0000148152.04401.20.

Melrose J, Roberts S, Smith S, et al. (2002). Increased nerve and blood vessel ingrowth associated with proteoglycan depletion in an ovine anular lesion model of experimental disc degeneration. Spine (Phila Pa 1976) 27:1278–85. doi:10.1097/00007632-200206150-00007.

Meng B, Grage SL, Babii O, et al. (2022). Highly fluorinated peptide probes with enhanced in vivo stability for 19F-MRI. Small 18:2107308. doi:10.1002/smll.202107308.

Meng FH, Shao XL, Song Y, Zhang T. (2017). Correlation between the expression of high temperature requirement serine protease A1 in nucleus pulposus tissue and the degree of intervertebral disc degeneration. Zhongguo Yi Xue Ke Xue Yuan Xue Bao 39:737–42. doi:10.3881/j.issn.1000-503X.2017.06.001.

Molinos M, Almeida CR, Caldeira J, et al. (2015). Inflammation in intervertebral disc degeneration and regeneration. J R Soc Interface 12:20141191. doi:10.1098/rsif.2014.1191.

Muttenthaler M, King GF, Adams DJ, Alewood PF. (2021). Trends in peptide drug discovery. Nat Rev Drug Discovery 20:309–25. doi:10.1038/s41573-020-00135-8.

Mwale F, Masuda K, Grant MP, et al. (2018). Short Link N promotes disc repair in a rabbit model of disc degeneration. Arthritis Res Ther 20:201. doi:10.1186/s13075-018-1625-9.

Normand G, Maker M, Penraat J, et al. (2020). Non-invasive molecular tracking method that measures ocular drug distribution in non-human primates. Commun Biol 3:16. doi:10.1038/s42003-019-0731-9.

Peters T, Kim S-W, Castro V, et al. (2017). Evaluation of polyesteramide (PEA) and polyester (PLGA) microspheres as intravitreal drug delivery systems in albino rats. Biomaterials 124:157–68. doi:10.1016/j.biomaterials.2017.02.006.

Petit A, Yao G, Rowas SA, et al. Effect of synthetic link N peptide on the expression of type I and type II collagens in human intervertebral disc cells. Tissue Eng Part A (2011). 17, 899–904 doi:10.1089/ten.tea.2010.0494.

Porter CJ, Charman SA. (2000). Lymphatic transport of proteins after subcutaneous administration. J Pharm Sci 89:297–310. doi:10.1002/(SICI)1520-6017(200003)89:3<297::AID-JPS2>3.0.CO;2-P.

Reum Son A, Kim DY, Hun Park S, et al. (2015). Direct chemotherapeutic dual drug delivery through intra-articular injection for synergistic enhancement of rheumatoid arthritis treatment. Sci Rep 5:14713. doi:10.1038/srep14713.

Richardson SM, Kalamegam G, Pushparaj PN, et al. (2016). Mesenchymal stem cells in regenerative medicine: focus on articular cartilage and intervertebral disc regeneration. Methods 99:69–80. doi:10.1016/j.ymeth.2015.09.015.

Roberts S, Urban JP, Evans H, Eisenstein SM. (1996). Transport properties of the human cartilage endplate in relation to its composition and calcification. Spine (Phila Pa 1976) 21:415–20. doi:10.1097/00007632-199602150-00003.

Roelofs PD, Deyo RA, Koes BW, et al. (2008). Non-steroidal anti-inflammatory drugs for low back pain. Cochrane Database Syst Rev 2008:CD000396. doi:10.1002/14651858.CD000396.pub3.

Roughley PJ. (2004). Biology of intervertebral disc aging and degeneration: involvement of the extracellular matrix. Spine (Phila Pa 1976) 29:2691–9. doi:10.1097/01.brs.0000146101.53784.b1.

Rudnik-Jansen I, Colen S, Berard J, et al. (2017). Prolonged inhibition of inflammation in osteoarthritis by triamcinolone acetonide released from a polyester amide microsphere platform. J Control Release 253:64–72. doi:10.1016/j.jconrel.2017.03.014.

Rudnik-Jansen I, Tellegen A, Beukers M, et al. (2019). Safety of intradiscal delivery of triamcinolone acetonide by a poly(esteramide) microsphere platform in a large animal model of intervertebral disc degeneration. Spine J 19:905–19. doi:10.1016/j.spinee.2018.10.014.

Rudnik-Jansen I, Tellegen AR, Pouran B, et al. (2019). Local controlled release of corticosteroids extends surgically induced joint instability by inhibiting tissue healing. Br J Pharmacol 176:4050–64. doi:10.1111/bph.14817.

Rustenburg CME, Emanuel KS, Peeters M, et al. (2018). Osteoarthritis and intervertebral disc degeneration: quite different, quite similar. JOR Spine 1:e1033. doi:10.1002/jsp2.1033.

Salo J, Mackiewicz Z, Indahl A, et al. (2008). Plasmin-matrix metalloproteinase cascades in spinal response to an experimental disc lesion in pig. Spine (Phila Pa 1976) 33:839–44. doi:10.1097/BRS.0b013e31816b1f1d.

Sélard E, Shirazi-Adl A, Urban JPG. (2003). Finite element study of nutrient diffusion in the human intervertebral disc. Spine (Phila Pa 1976) 28:1945–53; discussion 1953. discussion 1953 doi:10.1097/01.BRS.0000087210.93541.23.

Shi J, Liang Q, Zuscik M, et al. (2014). Distribution and alteration of lymphatic vessels in knee joints of normal and osteoarthritic mice. Arthritis Rheumatol 66:657–66. doi:10.1002/art.38278.

Simkin PA, Bassett JE. (2011). Pathways of microvascular permeability in the synovium of normal and diseased human knees. J Rheumatol 38:2635–42. doi:10.3899/jrheum.110785.

Sterner B, Harms M, Wöll S, et al. (2016). The effect of polymer size and charge of molecules on permeation through synovial membrane and accumulation in hyaline articular cartilage. Eur J Pharm Biopharm 101:126–36. doi:10.1016/j.ejpb.2016.02.004.

Suzuki H, Ura K, Ukeba D, et al. (2023). Injection of ultra-purified stem cells with sodium alginate reduces discogenic pain in a rat model. Cells 12:505. doi:10.3390/cells12030505.

Tellegen AR, Rudnik-Jansen I, Beukers M, et al. (2018). Intradiscal delivery of celecoxib-loaded microspheres restores intervertebral disc integrity in a preclinical canine model. J Control Release 286:439–50. doi:10.1016/j.jconrel.2018.08.019.

Tellegen AR, Rudnik-Jansen I, Pouran B, et al. (2018). Controlled release of celecoxib inhibits inflammation, bone cysts and osteophyte formation in a preclinical model of osteoarthritis. Drug Deliv 25:1438–47. doi:10.1080/10717544.2018.1482971.

Tiaden AN, Klawitter M, Lux V, et al. (2012). Detrimental role for human high temperature requirement serine protease A1 (HTRA1) in the pathogenesis of intervertebral disc (IVD) degeneration. J Biol Chem 287:21335–45. doi:10.1074/jbc.M112.341032.

Tryfonidou MA, de Vries G, Hennink WE, Creemers LB. (2020). "Old Drugs, New Tricks" - local controlled drug release systems for treatment of degenerative joint disease. Adv Drug Deliv Rev 160:170–85. doi:10.1016/j.addr.2020.10.012.

Tsitlanadze G, Machaidze M, Kviria T, et al. (2004). Biodegradation of amino-acid-based poly(ester amide)s: in vitro weight loss and preliminary in vivo studies. J Biomater Sci Polym Ed 15:1–24. doi:10.1163/156856204322752200.

Vos T, Allen C, Arora M, et al. (2016). Global, regional, and national incidence, prevalence, and years lived with disability for 310 diseases and injuries, 1990-2015: a systematic analysis for the Global Burden of Disease Study 2015. Lancet 388:1545–602. doi:10.1016/S0140-6736(16)31678-6.

Wagner EK, Vedadghavami A, Jacobsen TD, et al. (2020). Avidin grafted dextran nanostructure enables a month-long intra-discal retention. Sci Rep 10:12017. doi:10.1038/s41598-020-68351-1.

Wang Z, Hutton WC, Yoon ST. (2013). ISSLS prize winner: effect of link protein peptide on human intervertebral disc cells. Spine (Phila Pa 1976) 38:1501–7. doi:10.1097/BRS.0b013e31828976c1.

Weissleder R, Ntziachristos V. (2003). Shedding light onto live molecular targets. Nat Med 9:123–8. doi:10.1038/nm0103-123.

Whatley BR, Wen X. (2012). Intervertebral disc (IVD): structure, degeneration, repair and regeneration. Mater Sci Eng C 32:61–77. doi:10.1016/j.msec.2011.10.011.

Wiersema T, Tellegen AR, Beukers M, et al. (2021). Prospective evaluation of local sustained release of celecoxib in dogs with low back pain. Pharmaceutics 13:1178. doi:10.3390/pharmaceutics13081178.

Wilkinson DJ, Arques MDC, Huesa C, Rowan AD. (2019). Serine proteinases in the turnover of the cartilage extracellular matrix in the joint: implications for therapeutics. British J Pharmacology 176:38–51. doi:10.1111/bph.14173.

Willems N, Mihov G, Grinwis GCM, et al. (2017). Safety of intradiscal injection and biocompatibility of polyester amide microspheres in a canine model predisposed to intervertebral disc degeneration. J Biomed Mater Res B Appl Biomater 105:707–14. doi:10.1002/jbm.b.33579.

Yuan B, Rudeen K, Li J, et al. (2023). Biodegradable microspheres and hydrogel drug delivery system of Tumor Necrosis Factor (TNF) inhibitor and Growth Differentiation Factor 5 (GDF5) reduces disk inflammation in the rabbit model. Spine (Phila Pa 1976) 48:E257–65. doi:10.1097/BRS.0000000000004686.

Zhang YG, Guo TM, Guo X, Wu SX. (2009). Clinical diagnosis for discogenic low back pain. Int J Biol Sci 5:647–58. doi:10.7150/ijbs.5.647.

Zheng Q, Shen H, Tong Z, et al. (2021). A thermosensitive, reactive oxygen species-responsive, MR409-encapsulated hydrogel ameliorates disc degeneration in rats by inhibiting the secretory autophagy pathway. Theranostics 11:147–63. doi:10.7150/thno.47723.

Zhu Q, Gao X, Gu W. (2014). Temporal changes of mechanical signals and extracellular composition in human intervertebral disc during degenerative progression. J Biomech 47:3734–43. doi:10.1016/j.jbiomech.2014.09.004.